


Josephson Junctions with Artificial Superparamagnetic Barrier: A Promising Avenue for Nanoscale Magnetometry

Ivan P. Nevirkovets^{1,*}, Mikhail A. Belogolovskii^{1,2,3} and John B. Ketterson¹

¹*Department of Physics and Astronomy, Northwestern University, 2145 Sheridan Road, Evanston, Illinois 60208-3112, USA*

²*G.V. Kurdyumov Institute for Metal Physics, National Academy of Sciences of Ukraine, 36 Academician Vernadsky Boulevard., Kyiv, 03142, Ukraine*

³*Vasyl' Stus Donetsk National University, 21 600-richya Street, Vinnytsia, 21021, Ukraine*

 (Received 25 March 2020; revised 11 May 2020; accepted 2 June 2020; published 29 July 2020)

In this work, we realize a physical system—nanoengineered *singly connected* Josephson junction with a periodic superparamagnetic Ni/Al multilayer—that manifests supercurrent-versus-magnetic field response typical of a dc superconducting quantum interference device (SQUID); however, unlike a SQUID, which involves a superconducting loop occupying significant space, our lumped device is more suitable for miniaturization. In addition, we show that it exhibits enhanced magnetic field sensitivity as compared with conventional superconductor-insulator-superconductor Josephson junctions. SQUID-like oscillatory response to external magnetic fields, analogous to the two-slit optical interference, is explained in terms of the dominance of Andreev bound states localized at the barrier edges in the comparatively thick and strongly anisotropic weak links. Our results may lead to significant advancement in development of nanoscale magnetic sensing techniques applicable to individual molecules or magnetic nanoparticles.

DOI: [10.1103/PhysRevApplied.14.014092](https://doi.org/10.1103/PhysRevApplied.14.014092)

Recent advances in magnetic detection and imaging have led to significant progress in areas ranging from fundamental physics and chemistry to practical applications such as medical science and data storage. The drive to shrink the region being probed below the micron scale in order to sense strongly localized and very weak magnetic fields arising from individual molecules or magnetic nanoparticles requires alternative approaches to nanoscale magnetic field sensing.

Superconducting quantum interference devices (SQUIDs) are currently a commercial “gold standard” in weak-field magnetic sensing. By integrating the Josephson effect with the magnetic-flux quantization in superconducting rings, they represent one of the most striking manifestations of macroscopic quantum coherence in condensed matter. The need for nanoscale sensors has triggered the development of miniaturized SQUIDs aiming to combine high-sensitivity detection of very weak magnetic fields with nanometer-scale spatial resolution [1–4].

To improve the sensitivity and spatial resolution, the lateral dimensions of the detection loop of the SQUID should approach the size of the probed nanoparticle. In this case, the advantage of a conventional SQUID over a single Josephson junction (JJ) diminishes. When the size of

the superconducting loop shrinks, ultimately, the sensing area will be determined mainly by the London penetration depth, similarly to a single superconductor-insulator-superconductor (*S-I-S*) JJ. Therefore, at the nanoscale, a single JJ can compete as a sensitive magnetic field sensor [4–6]. Here we explore a promising junction design for nanoscale field sensing.

An ordinary *S-I-S* JJ is not suitable for this role because of the requirement that, at the operating temperature T , the Josephson energy $hI_c(T)/2e$ (where I_c is the Josephson critical current) should strongly exceed the thermal fluctuation energy $k_B T$. Estimates [4] show that, for $T \approx 4$ K, the critical current density, J_c , should be of the order of 10^9 A/m², which is hard to achieve with *S-I-S* junctions. The second problem is their significant capacitance leading to (i) hysteretic current-voltage characteristics that will interfere with optimal performance of nano-SQUIDs, and (ii) limitations of their high-frequency performance. Replacement of the insulating interlayer with a normal-metal (N) weak link allows for the required increase in J_c , intrinsic damping, and reduced capacitance.

The goal of this work is to propose a method to design a Josephson junction with normal (N) material providing maximum sensitivity to weak magnetic fields while maintaining a single-valued dependence of the critical current on the field. Enhancement of the field sensitivity can be achieved by using a magnetic material with a

*i-nevirkovets@northwestern.edu

high permeability as a barrier [7] or a part of the barrier [8]. In addition, the magnetic material should have zero coercivity to avoid hysteretic behavior, thus a superparamagnetic response is essential. Superparamagnetic materials are promising for many applications starting from magnetic field detectors [9–11] and memory [12] to stochastic computing [13]. To our knowledge, only a few publications report the use of superparamagnetic materials in Josephson junctions [7,8] to enhance their magnetic field sensitivity. Typically, these materials are alloys of different ferromagnets, or magnetic and nonmagnetic materials [7,9,10,12]. An approach reported in Ref. [8] and further developed in the present work is to use an *artificial superparamagnet* consisting of alternating nanolayers of a magnetic and a nonmagnetic metal; such an artificial superparamagnet potentially, allows for much greater flexibility in the choice of materials and tailoring the desired magnetic properties. This is especially important if one combines the superconducting and magnetic properties in the same device.

In the devices reported by Golod *et al.* [7], an increased field sensitivity is achieved not only by using a high-permeability material (Cu-Ni alloy), but also by exploiting the field-focusing effect. The latter, however, may pose a drawback if one is trying to achieve the highest spatial resolution. The devices reported by Nevirkovets and Mukhanov [8] are free from this drawback, and they manifested a higher field sensitivity (as measured by the magnetic field needed to form one period of the diffraction pattern for the same sensing area) than reported for typical Nb-based micro- or nano-SQUIDs [14–20], but they involved an insulating barrier, which, for very small JJ lateral dimensions, resulted in a low I_c . The aim of the present work is to demonstrate that the same oscillatory, SQUID-like, behavior of the $I_c(H)$ dependence is observed for small (approximately $1\ \mu\text{m}$ size) devices with an artificial superparamagnetic weak-link (WL) spacer that is a $(\text{Al}/\text{Ni})_n\text{Al}$ multilayer without any insulating barrier; owing to the absence of the insulating barrier, the devices have appreciable I_c magnitude. Moreover, we propose a theoretical model that explains the observed behaviors.

Here we consider devices patterned from Nb/ $(\text{Al}/\text{Ni})_{10}\text{Al}/\text{Nb}$ [$S-(N/F)_nN-S$] multilayer structures. The structures are deposited onto the oxidized Si substrates *in situ* using dc magnetron sputtering at room temperature. The thickness of the bottom and top Nb layers is 120 and 68 nm, respectively. The thicknesses of the Al and Ni layers, d_{Al} and d_{Ni} , composing the periodic $(\text{Al}/\text{Ni})_n$ structure are varied. In this work we describe the devices with $d_{\text{Al}}=3.1\ \text{nm}$ and $d_{\text{Ni}}=1.34\ \text{nm}$.

The multilayer pillars are patterned using optical lithography, reactive ion etching (RIE), Ar ion milling, and anodization followed by deposition of additional SiO_2 insulation. After deposition of a thick (approximately 300 nm) Nb wiring layer followed by

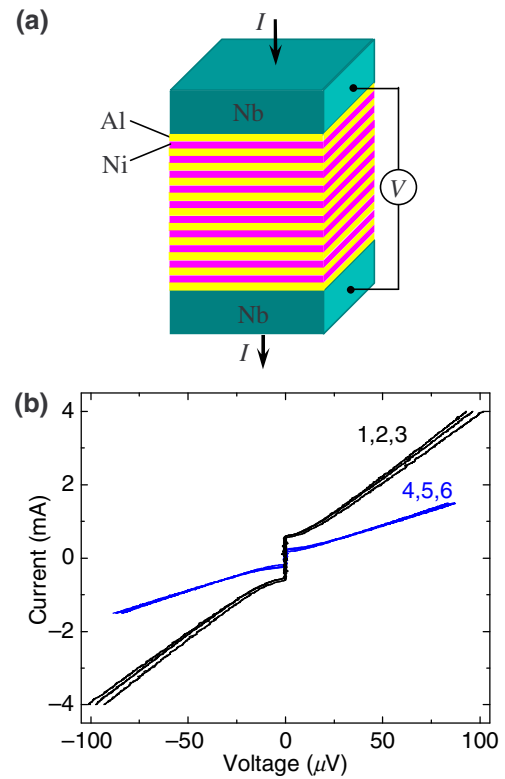


FIG. 1. (a) Schematic view of an $S-(N/F)_{10}N-S$ junction and (b) $I-V$ curves for three nominally identical $1.5 \times 1.5\ \mu\text{m}^2$ (black curves 1–3) and $0.9 \times 0.9\ \mu\text{m}^2$ (blue curves 4–6) $S-(NF)_{10}N-S$ devices with $S=\text{Nb}$, $N=\text{Al}$, $F=\text{Ni}$; $d_{\text{Al}}=3.10\ \text{nm}$, and $d_{\text{Ni}}=1.34\ \text{nm}$.

lift-off, the Josephson devices are formed for four-probe measurements. The lateral dimensions of the JJs are $1.5 \times 1.5\ \mu\text{m}^2$ and $0.9 \times 0.9\ \mu\text{m}^2$. A schematic view of the devices is shown in Fig. 1(a).

The samples are characterized at 4.2 K in a liquid He bath. Current-voltage characteristics ($I-V$ curves) of different Nb/ $(\text{Al}/\text{Ni})_{10}\text{Al}/\text{Nb}$ junctions are quite reproducible. Figure 1(b) illustrates this by showing the $I-V$ curves for three (nominally identical) $1.5 \times 1.5\ \mu\text{m}^2$ (black curves 1–3) and three $0.9 \times 0.9\ \mu\text{m}^2$ (blue curves 4–6) junctions. Note that the $I-V$ curves display supercurrents, indicating the presence of a long-range proximity effect in the $N-F$ multilayer [21].

In order to characterize the magnetic state of the Al/Ni multilayers, we fabricate a large area, $5.5 \times 11.4\ \text{mm}^2$, Nb/ $(\text{Al}/\text{Ni})_{70}$ sample on a Si/ SiO_2 substrate with $d_{\text{Al}}=3.10\ \text{nm}$ and $d_{\text{Ni}}=1.34\ \text{nm}$, and measured its magnetic moment M as a function of H applied parallel to the layers at 10 K, just above the critical temperature of Nb, $T_c \approx 9\ \text{K}$. The $M(H)$ dependence is shown in Fig. 2; it displays almost no hysteresis and saturates at $H \approx 2\ \text{kOe}$. The black squares, blue triangles, and red circles in Fig. 2 correspond to different sweeping directions of the magnetic

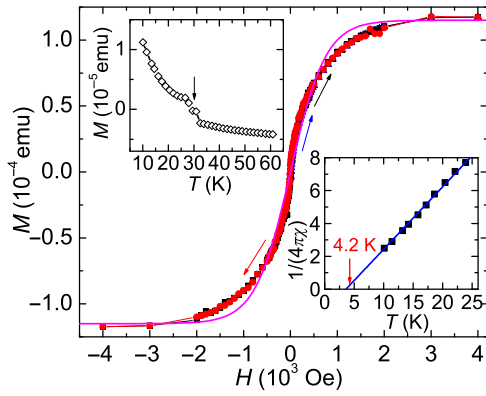


FIG. 2. Magnetic moment versus magnetic field dependence measured at 10 K for a periodic structure comprised of 70 Al/Ni periods with $d_{\text{Al}} = 3.1$ nm and $d_{\text{Ni}} = 1.34$ nm; the external magnetic field H is applied parallel to the layer planes. Black squares, blue triangles, and red circles correspond to different field-sweeping directions denoted by respective arrows. The magenta solid line is a fit of the experimental data to the form $M(H) = 1.15 \times 10^{-4} \tanh(13.3H)$ emu with H in kOe. The left inset shows $M(T)$ measured at $H = 500$ Oe in the field-cooled regime; note there is the signature of a magnetic transition at about 30 K as indicated by the arrow. The right inset shows the inverse dc susceptibility as a function of T below 30 K (squares) compared with a linear behavior (blue solid line) expected for the superparamagnetic regime.

field identified by the respective arrows. The $M(T)$ dependence measured at $H = 500$ Oe in the field-cooled (FC) regime indicates a transition from a diamagnetic response to a magnetically ordered state at about 30 K (see the left inset in Fig. 2). The data contain diamagnetic contribution from the Si/SiO₂ substrate [22]; since the temperature dependence of the susceptibility for diamagnetic materials is very weak, the diamagnetic background is subtracted from the magnetization data and the dependence of the inverse dc susceptibility, defined as $1/(4\pi\chi) \equiv H/M$, on T is calculated. It can be well fit by a straight line that intersects the horizontal axis at 3.6 K (see the right inset in Fig. 2). Note that at 4.2 K $4\pi\chi \approx 4.4$ and $\mu = 1 + 4\pi\chi \approx 5.4$. Therefore, the contribution of $4\pi M$ to the magnetic field B in the Al/Ni multilayer is several times greater than the external magnetic field H .

The linear behavior of the inverse dc susceptibility is consistent with a Curie-Weiss law $\chi(T) = C/(T - \theta)$ known to reflect a superparamagnetic behavior commonly exhibited by small clusters of a ferromagnetic material whose size is below some critical nm-scale diameter. If all the particles are identical, their easy axes are aligned with the applied field; at a low enough temperature, the magnetization of the assembly behaves as

$$M(H) = n\mu \tanh(\mu H / k_B T)$$

for $T > \theta$, where n and μ are the number density and magnetic moment of the nanoparticles in the sample, respectively. The main panel of Fig. 2 shows good agreement with this $M(H)$ behavior (magenta solid line).

From this fit, we can estimate the magnetic moment of a single Ni nanoparticle to be $\mu = 2.07 \times 10^{-19}$ emu, and knowing the bulk saturation magnetization of Ni, $M_s \sim 57.8$ emu/g, and the density, find the radius of our nanoparticles r . Such a rough estimate gives $r \sim 2.1$ nm in agreement with the thicknesses of the Ni films, as well as with the literature data for ultrathin Ni layers in the range below 2 nm [23] and for spherical Ni nanoparticles with a 2-nm radius at $T = 4.49$ K [24]. Hence, we conclude that our (Al/Ni)_{*n*}Al multilayer is in a superparamagnetic state. An advantage of using a superparamagnetic material is the absence of coercivity and remanent magnetization, which allows one to avoid magnetic hysteresis and associated losses.

Our S -(N/F)_{*n*} N - S Josephson junctions are unusual in that they display a supercurrent across the (N/F)_{*n*} N multilayer with a total thickness of about 50 nm, see Fig. 1(b). Indeed, the total thickness of the Ni layers in the samples, $d_{\Sigma\text{Ni}} = 13.4$ nm, significantly exceeds the induced coherence length ξ_{Ni} that is about 2 nm in our Ni films [25]. Although both $d_{\Sigma\text{Ni}}$ and ξ_{Ni} may be affected by possible interdiffusion of Al and Ni [26,27], we believe that, first of all, the relation $d_{\Sigma\text{Ni}} \gg \xi_{\text{Ni}}$ becomes possible due to superparamagnetic ordering in the (N/F)_{*n*} N system (see also related arguments in Ref. [23]). Such a configuration is not expected to support spin-triplet pairing; therefore, we suggest that the observed long-range proximity effect in our multilayered junctions is realized within a conventional singlet Cooper-pair framework. A second factor supporting superconducting correlations at such long distances is the proximity effect in Al interlayers [21].

We now focus on $I_c(H)$ dependences exhibited in Fig. 3(a) for our two types of JJs whose I - V curves are shown in Fig. 1(b). The open triangles (upper curves) are for the $1.5 \times 1.5 \mu\text{m}^2$ junction, whereas solid triangles and solid blue stars (lower curves) are for the $0.9 \times 0.9 \mu\text{m}^2$ junction. The $I_c(H)$ data displays typical dc SQUID characteristics, which distinguishes them from the Fraunhofer patterns of lumped junctions: in particular, (i) there is no difference between the width of the central lobe and the side lobes, and the ratios of the maxima positions in the $I_c(H)$ dependence are integers; (ii) the envelope function is smooth and decreases very slowly with increasing field; and (iii) a nonzero supercurrent is present at the minima, in contrast to the Fraunhofer pattern. The behavior of the SQUID-like oscillations may be slightly hysteretic when measured over a higher field interval, as shown by red and black solid triangles in Fig. 3(a) for a smaller junction; when measured over a smaller field interval ± 140 Oe, the $I_c(H)$ dependence for the same junction is nonhysteretic. In Fig. 3(b), we also show the $I_c(H)$ dependence calculated

according to the usual formula $I_c \propto |\sin(\pi \Phi / \Phi_0) / (\pi \Phi / \Phi_0)|$ for a $0.9 \times 0.9 \mu\text{m}^2$ Nb/Al/AIO_x/Nb junction (blue dashed line). In this calculation, we use a magnetic field penetration depth $\lambda_L = 91$ nm for our Nb films obtained from the experimental Fraunhofer pattern of a $10 \times 10 \mu\text{m}^2$ Nb/Al/AIO_x/Nb junction measured at 4.2 K. One can see that the period of this dependence is considerably larger than that obtained experimentally for the $0.9 \times 0.9 \mu\text{m}^2$ Nb/(Al/Ni)₁₀Al/Nb junction. We associate the smaller period of the $I_c(H)$ dependence in the junctions involving the N - F multilayer weak links with an enhancement of the magnetic flux in the multilayers that behave as artificial superparamagnets (by analogy with the artificial ferromagnets) [21]. Figure 3(b) shows the results of a theoretical simulation for the junctions involving N - F multilayers using a model described below.

In conventional JJs, the sensing area s can be estimated knowing the lateral size of the junction, w , and the effective magnetic thickness $t = d + 2\lambda_L$, where, d is the thickness of the oxide interlayer and λ_L is the London penetration depth [28]. For the samples with an (Al/Ni)₁₀Al WL, a modified term in the effective magnetic thickness appears [29]:

$$t' = \mu d + 2\lambda_L, \quad (1)$$

where d is the total thickness of Ni and Al nanolayers, $\mu = 1 + 4\pi\chi$ is the permeability averaged over the hybrid weak link, and $\lambda_L = 91$ nm. For our $1.5 \times 1.5 \mu\text{m}^2$ junction, using the period of $I_c(H)$ oscillations $\Delta H \approx 36$ Oe (cf. Fig. 3), and taking into account that $\Delta H = \Phi_0 / s'$ with $s' = wt'$ (see below), we obtain $\mu \approx 4.3$, implying a significant amplification of the magnetic field H by the artificial superparamagnetic medium inside the JJ. This value reasonably agrees with $\mu \approx 5.4$ obtained above from the analysis of the $M(T)$ dependence.

In order to explain an oscillatory $I_c(H)$ pattern in our junctions, we consider a model superconductor–normal–metal–superconductor (S - N - S) junction of width w and the WL thickness d ; see schematic of the device in Fig. 4(a). The dependence of I_c versus magnetic field, B , is then given by [28]:

$$I_c(B) = \max |I_s(B)| = \left| \int_{-\infty}^{\infty} J_c(y) \exp(2\pi i t' B y / \Phi_0) dy \right|. \quad (2)$$

A uniform distribution of the supercurrent density $J_c(y) = J_0 = \text{const}$ leads to the standard Fraunhofer interference pattern with the usual $|\sin(\pi \Phi / \Phi_0) / (\pi \Phi / \Phi_0)|$ form where the amplitude of the oscillations decays with the magnetic flux as Φ^{-1} , and the central lobe is twice as wide as the side lobes [28].

In order to explain the unconventional behavior of our junctions, we consider dephasing accumulated by an electron (or a hole) during its chaotic motion across an

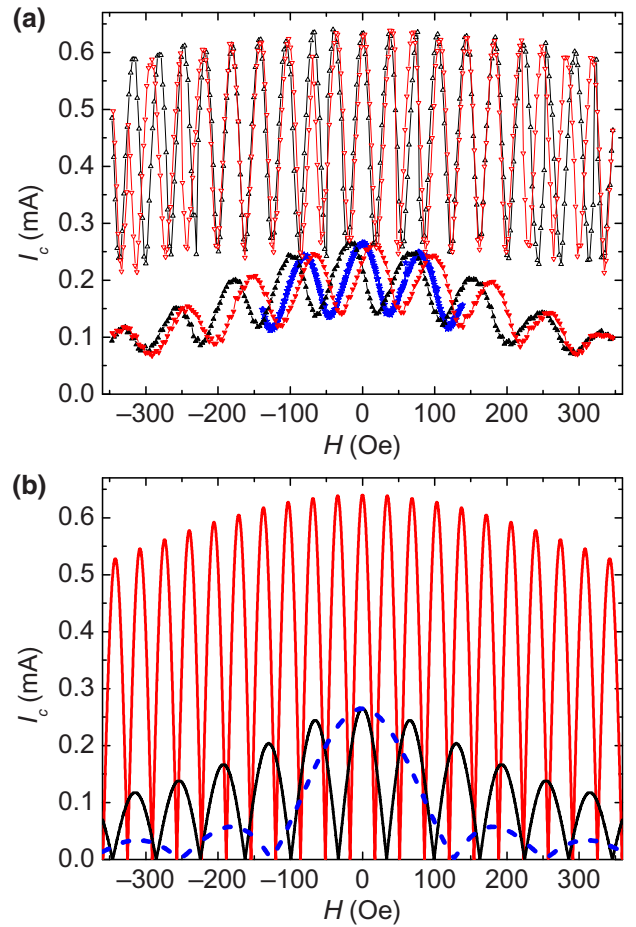


FIG. 3. (a) Representative $I_c(H)$ patterns for $1.5 \times 1.5 \mu\text{m}^2$ (open triangles, upper curves) and $0.9 \times 0.9 \mu\text{m}^2$ (solid triangles and stars, lower curves) Nb/(Al/Ni)₁₀Al/Nb devices whose I - V curves are shown in Fig. 1(b). Black and red symbols correspond to different directions of the magnetic field swept within a relatively high-field interval. The nonhysteretic dependence plotted with solid blue stars is for the $0.9 \times 0.9 \mu\text{m}^2$ device measured in a relatively low-field interval. (b) Theoretical simulations for the two types of Nb/(Al/Ni)₁₀Al/Nb Josephson junctions (red curve is for $1.5 \times 1.5 \mu\text{m}^2$ and black curve is for $0.9 \times 0.9 \mu\text{m}^2$ junctions), and for a $0.9 \times 0.9 \mu\text{m}^2$ Nb/Al/AIO_x/Nb Josephson junction having the same I_c magnitude as that for the smaller Nb/(Al/Ni)₁₀Al/Nb junction (blue dashed curve).

inhomogeneous WL. Electronic and transport properties of diffusive S - N - S structures in the presence of a perpendicular magnetic field attracted considerable attention. In wide diffusive junctions, several experiments have revealed a Fraunhofer-like $I_c(H)$ dependence in excellent agreement with the theory [28]. At the same time, in narrow junctions the magnetic interference pattern is replaced by a monotonic decay of the critical current with increasing fields [30]. The crossover from narrow-junction to wide-junction behavior was studied theoretically in Ref. [31] where it was shown that the magnetic length $\xi_B = \sqrt{\Phi_0 / B}$ sets the border between the two regimes. Aleiner *et al.*

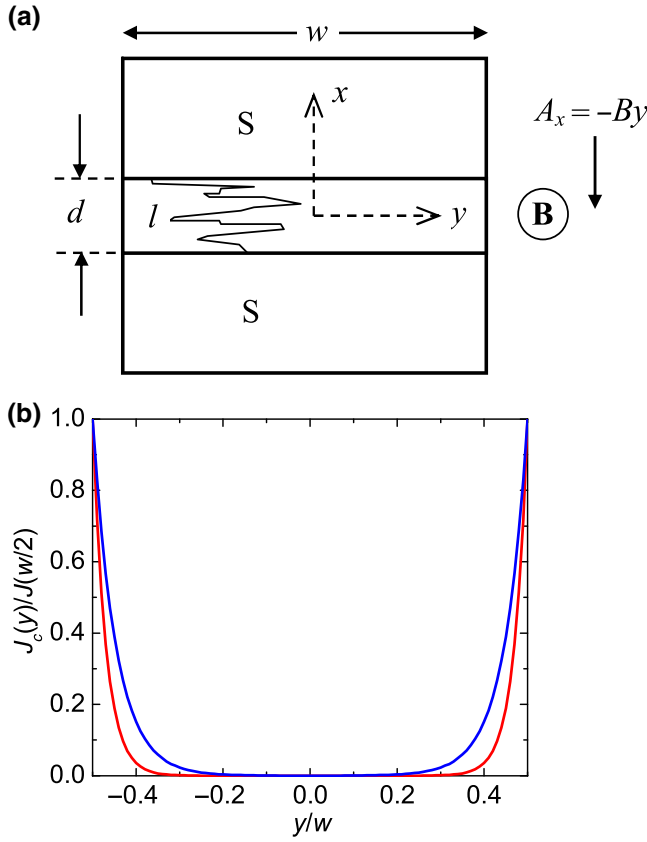


FIG. 4. (a) Schematics of the Josephson S - N - S junction with a diffusive weak link where the path length l strongly exceeds the distance d between the S electrodes. The x axis is directed perpendicular to the S - N interfaces which lie parallel to the y - z plane at $x = -d/2$ and $d/2$. The field \mathbf{B} is applied along the z axis and the vector potential is $\mathbf{A} = -By\hat{\mathbf{x}}$. The structure is translationally invariant along the z direction. (b) Supercurrent density profiles $J_c(y)$ for the two junctions with $w = 1.5 \mu\text{m}$ and $w = 0.9 \mu\text{m}$ (lower red and upper blue curves, respectively); the fitting parameter $l = 0.045 \mu\text{m}$ is used to fit measured $I_c(H)$ dependences [cf. Fig. 3(b)].

[32] analyzed quantum corrections to the probability of electron motion between two points in a singly connected diffusive conductor and found that the length scale ξ_B determines their strong spatial decay due to an unconstrained summation of a large number of rapidly oscillating contributions from different trajectories inside the bulk. At the same time, the presence of a nearby boundary imposes a sharp geometrical constraint on the allowed paths, which enhances the quantum interference effect. As a result, it gives rise to a type of Aharonov-Bohm oscillations, which reveal themselves in singly connected geometries due to the surface effects [32]. The role of the supercurrent localization near the edges of a diffusive Josephson junction was emphasized in Ref. [33]. The analysis [33] confirmed the presence of the damped-oscillating regime in wide samples where the junction width strongly exceeds the magnetic

length ξ_B [31]. The period of I_c versus B oscillations is found to be the same as that in the Fraunhofer interference pattern while the exponentially decaying factor resembled the damped regime for narrow junctions.

The above theoretical results [31–33] for diffusive Josephson junctions predict a decaying I_c versus B curves with or without oscillations, whereas in our junctions (cf. Fig. 3) the oscillations decay very weakly with increasing field. Hence, we believe we have a physical system where an alternative physical mechanism is at work, which is related to *strongly anisotropic* properties of our WLs. Such a system was not considered in previous theoretical studies.

The anisotropy, a key factor in our theoretical interpretation, arises due to the layered structure of the WL where the diffusion coefficient for the movement across the metallic layers, D_x , is much smaller than it is parallel to them, D_y . For an Andreev-bound state, the dephasing effect is characterized by the average $f(y) = \langle \exp(-i\phi) \rangle$ of the phase factor $\phi = (2\pi i/\Phi_0) \int \mathbf{A}(\mathbf{r}) d\mathbf{r}$ along all diffusive paths within the WL starting at the y coordinate, with \mathbf{A} being the vector potential. If y lies in the central part of the WL, a huge number of contributions with random signs largely cancel each other, and for a given diffusive time τ yield

$$\begin{aligned} & \left\langle \exp \left(-\frac{2\pi i}{\Phi_0} \int \mathbf{A}(\mathbf{r}) d\mathbf{r} \right) \right\rangle \\ &= \left\langle \exp \left(-\frac{1}{2} \left(\frac{2\pi}{\Phi_0} \int \mathbf{A}(\mathbf{r}) d\mathbf{r} \right)^2 \right) \right\rangle \\ &= \exp \left(-\frac{\pi^2 D_y B^2 d^2 \tau}{3\Phi_0^2} \right) = \exp \left(-\frac{\tau}{\tau_B} \right) \end{aligned} \quad (3)$$

with $\tau_B = 3\Phi_0^2/(\pi^2 D_y d^2 B^2)$. The probability to cross the WL in a fixed time τ is proportional to $\exp[-d^2/(4D_x\tau)]$, thus finally we find that $\langle \exp(-2\pi i/\Phi_0) \int \mathbf{A}(\mathbf{r}) d\mathbf{r} \rangle$ is proportional to $\exp(-d^2/\tilde{\xi}_B^2)$ with $\tilde{\xi}_B^2 = \xi_B^2/\sqrt{D_y/D_x} = \Phi_0/(\sqrt{D_y/D_x}B)$. Hence, similarly to results of Ref. [32], the current in the central part of the WL can be strongly suppressed by the randomness when the WL thickness is relatively large and the condition $D_y \gg D_x$ is satisfied. Let us stress again that in a strongly anisotropic WL the characteristic length $\tilde{\xi}_B$ replaces the well-known ξ_B value and that the SQUID-like oscillations are arising when $w \gg \tilde{\xi}_B$.

In contrast to the *central* part of the WL, the current survives for electron trajectories confined to its edges. Indeed, for the near-edge trajectories, the integration in Eq. (3) is only one sided [over $\delta y > -w/2$ or $\delta y < w/2$ at the left (right) boundary]. In this case, the near-edge currents are not as strongly suppressed as those in the WL central region. A more precise analysis would depend on the scattering processes from the boundaries. For the main part

of near-surface trajectories, we are dealing with a power-law decay while “skipping orbit” trajectories shown in Fig. 1(d) of the paper [32] result in an exponential decay that is weaker than that in Eq. (3). Since our knowledge of charge scattering from edges is limited, we restrict ourselves to a phenomenological model that postulates an edge-dominated transport within the near-edge region.

As an oversimplified model for our qualitative discussion, we assume that the current varies along w as $J_c(y) = \text{const} \left| \int_{-w/2}^{w/2} J_0 \sinh[\pi(y - y')/2l] dy' \right|$, where l is an average decay length in the y direction. For $d \ll w$, the $I_c(\Phi)$ pattern can be found using Eq. (2).

In Fig. 4(b) we plot two spatially dependent $J_c(y)$ curves used for the simulations shown in Fig. 3(b). The curves are calculated for $w = 0.9 \mu\text{m}$ and $w = 1.5 \mu\text{m}$ using l as a fitting parameter; for $l = 0.045 \mu\text{m}$, we obtain the best fit to both experimental $I_c(H)$ dependences in Fig. 3(a). The calculations are performed using the effective magnetic thickness l' with $d = 47.5 \text{ nm}$, $\mu \approx 5.4$, and $\lambda_L = 91 \text{ nm}$ in Eq. (1) and the two w values. Results of the $I_c(H)$ simulations, where amplitudes of the calculated dependences are adjusted to respective experimental I_c values, are shown in Fig. 3(b) together with the standard Fraunhofer pattern for an S - I - S junction with $w = 0.9 \mu\text{m}$. The period and general character of the measured $I_c(H)$ curves are well reproduced by our oversimplified model.

Note that in the experimental $I_c(H)$ dependences, the oscillations discussed above are superposed over a broad background observed in all studied samples. Similar quasi-Gaussian decay of the critical current with field has been predicted [31,33] and observed [30] for long narrow JJs with Ag nanowires coupling superconducting electrodes. Earlier, it was shown theoretically [34,35] that, for the coherent regime, the total dc current in a symmetric two-barrier JJ is given by the integration of a single-channel result over the distribution function peaked at the barrier transmission coefficients $D = 0$ and $D = 1$. We suggest that similar situation may take place in our multilayer structure; i.e., the presence of the high-transmission narrow channels with $D \sim 1$ generates a quasi-Gaussian broad contribution to the $I_c(H)$ dependence, while the rest of the channels are responsible for oscillations discussed above. Clearly, this matter requires further investigation.

The proposed devices overcome the main obstacles on the way towards application of *single* Josephson junctions in nanoscale magnetometry. First, J_c is only slightly below the required value [4] of about 10^9 A/m^2 needed to overcome thermal fluctuations in nanoscale JJs at an operating temperature of several kelvins. For our Nb/(AlNi)₁₀Al/Nb devices, we estimate J_c to be about $0.3 \cdot 10^9 \text{ A/m}^2$. Further optimization is required for obtaining the desired value of J_c . Another requirement [4], a nonhysteretic current-voltage characteristic, is realized in our devices as well [cf. Fig. 1(b)]. The reason for this is that our devices

are intrinsically shunted JJs with strongly disordered local weak-link transmission probabilities being tiny for the main (internal) part of the JJ, whereas a small part of the interface is well transparent [35]. Because of the absence of an insulating WL, our devices have small capacitance. The superparamagnetic property of the WL allows us to enhance the field sensitivity and, simultaneously, to avoid the hysteresis. An important innovation is using an artificial superparamagnet for WL, which, potentially, allows for flexibility in design of magnetic properties and for a broader choice of materials not only for development of magnetic JJs, but also for other applications. When using JJs as magnetic sensors, increasing the number of magnetic layers in our devices may lead to improvement of the field sensitivity, but also to adverse reduction of the I_c magnitude. Our theoretical model suggests that the solution may be to deposit thin conductive (or superconductive) layers onto the two opposite edges of the N - F stack, thereby providing the two edge channels for the supercurrent.

In conclusion, the hybrid S - $(N/F)_n$ - N - S devices proposed in this work have the potential to replace ordinary dc SQUIDs in the nanoscale magnetometry, since they are much more suitable for miniaturization and for detection of low magnetic fields from nanosize objects, as well as for the development of other devices exploiting quantum interference effects.

ACKNOWLEDGMENTS

The authors thank O. Chernyashevskyy and A. Strom for technical assistance and O. A. Mukhanov for useful discussions. M. Belogolovskii acknowledges support from the Fulbright Visiting Scholar Program and the Fundamental Research Programme funded by the Ministry of Education and Science of Ukraine (Project No. 0120U102059). Later stages of this research received support from NSF Grant No. DMR 1905742.

-
- [1] C. P. Foley and H. Hilgenkamp, Why NanoSQUIDs are important: An introduction to the focus issue, *Supercond. Sci. Technol.* **22**, 064001 (2009).
 - [2] C. Granata and A. Vettoliere, Nano superconducting quantum interference device: A powerful tool for nanoscale investigations, *Phys. Rep.* **614**, 1 (2015).
 - [3] M. J. Martínez-Pérez and D. Koelle, NanoSQUIDs: Basics & recent advances, *Phys. Sci. Rev.* **2**, 20175001 (2017).
 - [4] J. Gallop and L. Hao, in *Fundamentals and Frontiers of the Josephson Effect*, (Springer Nature Switzerland, Cham, Switzerland, 2019), pp. 555.
 - [5] B. L. Plourde and D. J. Van Harlingen, Design of a scanning Josephson junction microscope for submicron-resolution magnetic imaging, *Rev. Sci. Instrum.* **70**, 4344 (1999).
 - [6] A. Nakayama, Y. Nishi, N. Watanabe, S. Abe, and Y. Okabe, Measurement of trapped flux magnetic field near the

- superconducting film by the dependence of superconducting current through a Josephson junction sensor, *J. Phys. Conf. Ser.* **234**, 042023 (2010).
- [7] T. Golod, O. M. Kapran, and V. M. Krasnov, Planar Superconductor-Ferromagnet-Superconductor Josephson Junctions as Scanning-Probe Sensors, *Phys. Rev. Appl.* **11**, 014062 (2019).
- [8] I. P. Nevirkovets and O. A. Mukhanov, Peculiar interference pattern of Josephson junctions involving periodic ferromagnet-normal metal structure, *Supercond. Sci. Technol.* **31**, 03LT01 (2018).
- [9] R. P. Cowburn, D. K. Koltsov, A. O. Adeyeye, and M. E. Welland, Sensing magnetic fields using superparamagnetic nanomagnets, *J. Appl. Phys.* **87**, 7082 (2000).
- [10] Y. Jang, C. Nam, J. Y. Kim, B. K. Cho, Y. J. Cho, and T. W. Kim, Magnetic field sensing scheme using CoFeB/MgO/CoFeB tunneling junction with superparamagnetic CoFeB layer, *Appl. Phys. Lett.* **89**, 163119 (2006).
- [11] Y. Cao, P. Kumar, Y. Zhao, Y. Suzuki, S. Yoshimura, and H. Saito, High magnetization Co-GdO_x superparamagnetic granular films as magnetic coating materials for high-sensitivity alternating magnetic force microscopy tip, *J. Magn. Magn. Mater.* **462**, 119 (2018).
- [12] R. Schad, H. Alouach, J. W. Harrell, M. Shamsuzzoha, and D. Wang, Superparamagnetic NiFeCo layers as free layers in magnetic tunnel junctions, *J. Appl. Phys.* **93**, 8561 (2003).
- [13] M. W. Daniels, A. Madhavan, P. Talatchian, A. Mizrahi, and M. D. Stiles, Energy-efficient Stochastic Computing with Superparamagnetic Tunnel Junctions, *Phys. Rev. Appl.* **13**, 034016 (2020).
- [14] V. Bouchiat, M. Faucher, C. Thirion, W. Wernsdorfer, T. Fournier, and B. Pannetier, Josephson junctions and superconducting quantum interference devices made by local oxidation of niobium ultrathin films, *Appl. Phys. Lett.* **79**, 123 (2001).
- [15] M. Faucher, T. Fournier, B. Pannetier, C. Thirion, W. Wernsdorfer, J. C. Villegier, and V. Bouchiat, Niobium and niobium nitride SQUIDS based on anodized nanobridges made with an atomic force microscope, *Physica C* **368**, 211 (2002).
- [16] J.-P. Cleuziou, W. Wernsdorfer, V. Bouchiat, T. Ondarcuhu, and M. Monthieux, Carbon nanotube superconducting quantum interference device, *Nat. Nanotechnol.* **1**, 53 (2006).
- [17] D. Hazra, J. R. Kirtley, and K. Hasselbach, Nano-superconducting quantum interference devices with continuous read out at milliKelvin temperatures, *Appl. Phys. Lett.* **103**, 093109 (2013).
- [18] D. Vasyukov, Y. Anahory, L. Embon, D. Halbertal, J. Cuppens, L. Neeman, A. Finkler, Y. Segev, Y. Myasoedov, M. L. Rappaport, M. E. Huber, and E. Zeldov, A scanning superconducting quantum interference device with single electron spin sensitivity, *Nat. Nanotechnol.* **8**, 639 (2013).
- [19] R. Russo, E. Esposito, A. Crescitelli, E. Di Gennaro, C. Granata, A. Vettoliere, R. Cristiano, and M. Lisitskiy, NanoSQUIDS based on niobium nitride films, *Supercond. Sci. Technol.* **30**, 024009 (2017).
- [20] S. Biswas, C. B. Winkelmann, H. Courtois, and A. K. Gupta, Josephson coupling in the dissipative state of a thermally hysteretic μ -SQUID, *Phys. Rev. B.* **98**, 174514 (2018).
- [21] S. V. Bakurskiy, M. Yu. Kupriyanov, A. A. Baranov, A. A. Golubov, N. V. Klenov, and I. I. Soloviev, Proximity effect in multilayer structures with alternating ferromagnetic and normal layers, *JETP Lett.* **102**, 586 (2015).
- [22] J. Philip, A. Punnoose, B. I. Kim, K. M. Reddy, S. Layne, J. O. Holmes, B. Satpati, P. R. Leclair, T. S. Santos, and J. S. Moodera, Carrier-controlled ferromagnetism in transparent oxide semiconductors, *Nat. Mater.* **5**, 298 (2006).
- [23] C. A. Neugebauer, Saturation magnetization of nickel films of thickness less than 100 Å, *Phys. Rev.* **116**, 1441 (1959).
- [24] J. Singh, T. Patel, N. Kaurav, and G. S. Okram, in *AIP Conference Proceedings*, AIP Publishing LLC: Melville, NY, (2016), 1731, pp. 050036.
- [25] I. P. Nevirkovets, O. Chernyashevskyy, G. V. Prokopenko, O. A. Mukhanov, and J. B. Ketterson, Control of supercurrent in hybrid Superconducting/Ferromagnetic transistors, *IEEE Trans. Appl. Supercond.* **25**, 1800705 (2015).
- [26] G. Dorey, The growth of thin nickel films on a (111) aluminium surface, *Thin Solid Films* **5**, 69 (1970).
- [27] S. Singh, S. Basu, M. Gupta, C. F. Majkrzak, and P. A. Kienzle, Growth kinetics of intermetallic alloy phase at the interfaces of a Ni/Al multilayer using polarized neutron and x-ray reflectometry, *Phys. Rev. B.* **81**, 235413 (2010).
- [28] A. Barone and G. Paterno, *Physics and Applications of the Josephson Effect* (Wiley, Hoboken, NJ, 1982).
- [29] G. Wild, C. Probst, A. Marx, and R. Gross, Josephson coupling and Fiske dynamics in ferromagnetic tunnel junctions, *Eur. Phys. J. B.* **78**, 509 (2010).
- [30] A. Murani, S. Sengupta, A. Kasumov, R. Deblock, C. Celle, J.-P. Simonato, H. Bouchiat, and S. Guéron, Long- to short-junction crossover and field-reentrant critical current in Al/Ag-nanowires/Al Josephson junctions, arXiv:1911.02962 [cond-mat.mes-hall] (2019).
- [31] J. C. Cuevas and F. S. Bergeret, Magnetic Interference Patterns and Vortices in Diffusive SNS Junctions, *Phys. Rev. Lett.* **99**, 217002 (2007).
- [32] I. L. Aleiner, A. V. Andreev, and V. Vinokur, Aharonov-Bohm Oscillations in Singly Connected Disordered Conductors, *Phys. Rev. Lett.* **114**, 076802 (2015).
- [33] B. Crousy and D. A. Ivanov, Magnetic interference patterns in long disordered Josephson junctions, *Phys. Rev. B.* **87**, 024514 (2013).
- [34] A. Brinkman and A. A. Golubov, Coherence effects in double-barrier Josephson junctions, *Phys. Rev. B.* **61**, 11297 (2000).
- [35] M. Belogolovskii, E. Zhitlukhina, V. Lacquaniti, N. De Leo, M. Fretto, and A. Soso, Intrinsically shunted Josephson junctions for electronics applications, *Low Temp. Phys.* **43**, 756 (2017).